Vol. 718: 23–37, 2023
https://doi.org/10.3354/meps14391

MARINE ECOLOGY PROGRESS SERIES
Mar Ecol Prog Ser

Published September 7

Uptake of excess phosphate at low inorganic N:P ratio in a coastal sea afflicted with eutrophication

Mari Vanharanta[1,2,*], Kristian Spilling[2,3]

[1]Tvärminne Zoological Station, University of Helsinki, 10900 Hanko, Finland
[2]Marine and Freshwater Solutions, Finnish Environment Institute, 00790 Helsinki, Finland
[3]Centre for Coastal Research, University of Agder, 4630 Kristiansand, Norway

ABSTRACT: Following the spring bloom in the northern Baltic Sea, nitrogen limits phytoplankton growth and there is typically a residual phosphate concentration (>0.2 µmol l^{-1}) remaining that is often assumed to induce the recurring blooms of nitrogen-fixing cyanobacteria. However, these cyanobacterial blooms typically occur 2–3 mo later during the summer, when the phosphate concentration has been depleted, and it is unclear what organisms take up the excess phosphate. We studied the removal potential of excess phosphate (0.55 µmol l^{-1}) at different temperatures (10, 13, 16°C) and with or without nitrogen addition in an indoor 20 l tank experiment. In addition, we followed the element pools and plankton community composition. As expected, the phosphate uptake rate was up to 3-fold faster in nitrogen-amended than non-amended tanks, but complete drawdown of phosphate also occurred under severe nitrogen limitation. The uptake ratio of dissolved inorganic nitrogen to phosphorus was 4.6, which is substantially lower than the Redfield ratio (16) and indicates excessive phosphate removal potential relative to nitrogen. A large part of the excess phosphate ended up in the particulate pool, which has a higher potential to sink out from the surface. The nitrogen-fixing cyanobacteria *Nodularia spumigena* grew close to summer bloom concentrations only in the highest experimental temperature. However, the combined biovolume of all 3 major bloom-forming cyanobacteria accounted for only 5.3% of the total autotropic biovolume, and their potential phosphate uptake was calculated to be <3% of the excess phosphate available at the beginning of the study. Therefore, our results demonstrate that the contribution of filamentous cyanobacteria to the removal of excess phosphate is small.

KEY WORDS: Baltic Sea · Excess phosphate uptake · Post-spring-bloom · Cyanobacteria · *Nodularia spumigena*

1. INTRODUCTION

Despite successful local reductions in nutrient inputs into the Baltic Sea, eutrophication remains the largest threat to this fragile ecosystem (Murray et al. 2019). The largest periods of new production are the annual spring blooms and, in some areas, the blooms of diazotrophic cyanobacteria. The spring bloom is based on new production, which consumes the inorganic nutrients available after wintertime mixing, and a significant fraction of this biomass settles to the seafloor after the depletion of inorganic nitrogen (Lignell et al. 1993, Heiskanen 1998). Nitrogen limitation of the spring bloom is evident in large parts of the Baltic Sea, and excess phosphate, up to 0.6 µmol l^{-1}, remains in the Gulf of Finland and the Baltic Proper after available nitrate (NO_3^-) has been depleted (Spilling et al. 2018).

Degradation of the settled biomass drives the formation of hypoxic and anoxic bottom areas (Kupari-

*Correspondence: mari.vanharanta@syke.fi

Publisher: Inter-Research · www.int-res.com

nen & Tuominen 2001, Conley 2012), which further contribute to the low dissolved inorganic nitrogen to phosphorus ratio (DIN:DIP), as under anoxic sediment conditions, iron-bound phosphorus is mobilized at the reductive water–sediment interface, causing the release of phosphate from the sediment into the water (Pitkänen et al. 2001, Stigebrandt et al. 2014, Lehtoranta et al. 2017). This process counteracts the reductions of external nutrient inputs, as its input exceeds the loading from land in parts of the Baltic Sea (Conley et al. 2002).

A low DIN:DIP ratio gives a competitive advantage to diazotrophic cyanobacteria capable of fixing atmospheric nitrogen (N_2), whereas other functional groups are limited by its more accessible forms (Niemi 1979). However, the new bioavailable nitrogen produced by cyanobacteria supports production of other organisms on several trophic levels by alleviating the nitrogen limitation during summer (Karlson et al. 2015). The main bloom period of the generally slow-growing diazotrophic cyanobacteria usually starts in July, when the ratio of solar irradiation to the mixed-layer depth is optimal for their growth (e.g. Schneider et al. 2014). This is approximately 2 mo after the end of the spring bloom in the Northern Baltic Proper and the Gulf of Finland. By this time, the excess phosphate has been depleted, suggesting that the cyanobacteria have either taken up large quantities as internal storage available for several cell divisions or, alternatively, other organisms have taken up the phosphate and other phosphorus sources are required for the massive late summer cyanobacteria blooms (Nausch et al. 2008, Raateoja et al. 2011, Wasmund et al. 2012, Löptien & Dietze 2022). Thus, the relationship between excess phosphate and cyanobacteria growth is still unclear and requires additional experimental and observational data (Munkes et al. 2021).

Microorganisms utilize inorganic nutrients in specific ratios depending on, e.g. their biochemical composition. For example, the cellular elemental content of heterotrophic bacteria generally requires more phosphorus than nitrogen compared to phytoplankton, resulting in a significantly lower DIN:DIP uptake ratio than the canonical Redfield ratio of 16:1 (Kirchman 1994), whereas eukaryotic phytoplankton have higher stoichiometric plasticity and nutrient storage capacities compared to prokaryotes (Tanioka & Matsumoto 2020). In addition, temperature is an important factor regulating cellular biochemical reactions (Boscolo-Galazzo et al. 2018), and it alters cellular elemental stoichiometry by, e.g. increasing the particulate organic carbon to nitrogen ratio in algae due to enhanced carbon fixation (Moorthi et al. 2016). Small osmotrophs are strong competitors under nutrient-limiting conditions because of their high surface-to-volume ratio. Alternatively, mixotrophy can be advantageous under nutrient-poor conditions (Lagus et al. 2004). Thus, in addition to cyanobacteria, nitrogen limitation after the spring bloom could select for small-sized heterotrophic bacteria and autotrophic picoplankton cells or mixotrophic organisms.

In this study, we investigated the potential for excess phosphate removal by the post-spring-bloom plankton (pico, nano, and micro) community. Our primary objectives were to determine how rapidly phosphate is taken up under different temperatures, what group of plankton takes up the phosphate, and in what form the phosphorus ends up. We hypothesized that pico-sized organisms take up most of the excess phosphate after nitrogen sources have been depleted, whereas nanophytoplankton take up more of the phosphate when NO_3^- is available. In addition, we hypothesize that most of the phosphate is depleted before the filamentous cyanobacteria start to grow.

2. MATERIALS AND METHODS

2.1. Sampling and experimental setup

We collected seawater with a Limnos sampler from 5 m depth at Längden (59° 46′ 37″ N, 23° 15′ 1″ E) in the outer Tvärminne Archipelago. Samples were collected on 24 April 2019, during a period that typically represents the start of the post-spring-bloom phase, when the depletion of inorganic nitrogen has terminated the spring bloom. The water was pre-screened through a 50 µm mesh into pre-cleaned (HCl and deionized water) 20 l experimental tanks. Temperature (°C), salinity, and dissolved oxygen (mg O_2 l^{-1}) were measured using a portable calibrated digital water meter (MU 6100 H, VWR). The tanks were covered at all times to prevent light shock and were placed in the dark at 5°C overnight after the return to the accredited laboratory of the Tvärminne Zoological Station.

On the day we collected the water, surface DIN concentration was already below the detection limit, but there was an excess phosphate of 0.15 µmol l^{-1} in the surface water. The chlorophyll *a* (chl *a*) concentration was 11 µg l^{-1}, and the phytoplankton net sample collected on site was dominated by a single-celled dinoflagellate, most likely *Biecheleria baltica*

(Sundström et al. 2010). Surface temperature and salinity were 5.2°C and 5.8, respectively, and a characteristic seasonal thermocline had started to form at ~10 m depth. The initial particulate C:N ratio was slightly higher (8.8) than the Redfield value (6.6).

The following morning, on 25 April, phosphate (KH_2PO_4) was added in all units to a starting concentration of 0.55 µmol l^{-1}, and the units were distributed into temperature-controlled climate chambers. The units were exposed to full-spectrum light with daylight fluorescent tubes (Aquarius plant LED, AB Aqua Medic) with a 16 h light:8 h dark cycle and irradiance of ~50 µmol m^{-2} s^{-1} corresponding to ~5 m depth. The tanks were aerated with 0.2 µm filtered air, providing air-equilibrated CO_2 concentration and turbulence, keeping cells in suspension.

The first sampling occurred on 25 April, marking experiment Day 1. After this, we took samples on experiment Days 5, 8, 12, 15, 19, 22, 26, 29, 33, and 35 (29 May). Sampling on the last day (Day 35) involved more rigorous shaking and included more of the sedimented material compared to the regular samplings. Therefore, the data exploration of Day 35 mainly concentrates on the particulate organic nutrients and the total phosphorus pool.

The experimental setup consisted of a control with no further treatment and a treatment with added nitrogen in the form of NO_3^-. The 2 treatments were replicated (n = 3) across a temperature gradient of 10 ± 0.5, 13 ± 0.5, and 16 ± 0.5°C. This was done instead of replicating one temperature, with the rationale of recording the variability within this temperature range, which is typical during May–June in the study area. A concentration of 0.84 µmol NO_3^- l^{-1} was added after each of the 10 samplings to total a cumulative addition of 8.4 µmol NO_3^- l^{-1} at the end of the experiment instead of a one-off addition of NO_3^- at the beginning. This simulated small mixing events, which are frequent in the study area during spring (Spilling 2007) and corresponded a DIN:DIP ratio of 16. The bottles were gently stirred with a polycarbonate rod before each sampling and after nutrient addition.

2.2. Inorganic nutrients and dissolved and particulate organic nutrients

DIN (including NO_3^-+NO_2^- and NH_4^+), DIP (PO_4^{3-}), and dissolved silicate (DSi; including SiO_2) were determined according to Grasshoff et al. (1999).

For dissolved organic carbon (DOC) and total dissolved nitrogen (TDN) analyses, 20 ml of sample was filtered into acid-washed and pre-combusted glass vials through 0.2 µm polycarbonate syringe filters (Whatman) and acidified with 2 M HCl. Concentrations of DOC and TDN were determined using a Shimadzu TOC-VCPH analyzer equipped with a chemiluminescence detector (Shimadzu TNM-1) for measuring TDN. Dissolved organic nitrogen (DON) was calculated by subtracting DIN from TDN. Total dissolved phosphorus (TDP) concentration was determined by filtering 30 ml of sample through 0.2 µm polycarbonate syringe filters (Whatman) into acid-washed centrifuge tubes, according to Koistinen et al. (2017). Dissolved organic phosphorus (DOP) was obtained from the difference between TDP and DIP.

For particulate organic carbon (POC), nitrogen (PON), and phosphorus (POP), 100 ml of sample was filtered in duplicates onto acid-washed (2 M HCl) and pre-combusted (450°C, 4 h) GF/F filters (Whatman). POC and PON filters were dried at room temperature before measurements with a CHN element analyzer coupled to a mass spectrometer (Europa Scientific). POP was determined according to Solórzano & Sharp (1980), with slight modification by Koistinen et al. (2017). Particulate organic elemental ratios (POC:PON:POP) were calculated on a molar basis.

2.3. Chl *a* and biogenic silica

Chl *a* concentration was determined in duplicates by filtering 100 ml of sample onto GF/F filters with a nominal pore size of ~0.7 µm (Whatman) and extracted with 10 ml of 94% ethanol in the dark at room temperature for 24 h before analysis with a fluorometer (Varian, Cary Eclipse). Chl *a* measurements were calibrated with pure chl *a* (Sigma). Biogenic silica (BSi) concentration was determined by filtering 50 ml of sample in duplicates onto 0.8 µm polycarbonate membrane filters (DHI) and measured according to Koistinen et al. (2018).

2.4. Plankton community

Abundances of heterotrophic bacteria (hereafter bacteria) and *Synechococcus*-like picocyanobacteria cells were examined from samples preserved in paraformaldehyde (1% final concentration) for 15 min in darkness and stored at −80°C until further analysis according to Gasol & Del Giorgio (2000). Samples were stained with the nucleic acid stain

SYBRGreen I (Molecular Probes) at a 10^{-4} (v/v) concentration for 15 min in the dark, and bacteria were counted by flow cytometry (LSR II, BD Biosciences). To estimate the counting volume, fluorescent Countbright absolute counting beads (Thermo Fisher Scientific) were added to all samples. The gating of bacteria was done according to their side scatter (SSC) and green fluorescence using FACSDiva Software (BD Biosciences). For the characterization of *Synechococcus*-like cyanobacteria cells, red fluorescence (chl *a*) and green fluorescence were used according to Gasol & Del Giorgio (2000). This cluster likely includes mainly picocyanobacteria, as they were close to the size range of the beads (0.5–1 µm diameter) and picoeukaryotes would typically appear in the range larger than 1 µm (Alegria Zufia et al. 2021). All counts were obtained using Flowing Software 2.5.1 (https://bioscience.fi/?s=flowing+software).

The abundances of picoeukaryotes and nanophytoplankton were determined from live samples with a flow cytometer (Partec Cube 8, Sysmex Partec) equipped with 2 Argon lasers (488 and 561 nm excitation light). The volume counted was 800 µl, and different populations were identified according to their forward scatter, SSC, and pigment fluorescence (chl *a*, phycoerythrin). A group of particles with low chl *a*, low SSC, and little to no phycoerythrin signal was characterized as picoeukaryotes. The nanophytoplankton population stood out with higher SSC and chl *a* fluorescence than the picoeukaryotes. Data were analyzed with FCS Express v.7 software (De Novo).

Nano- and microplankton samples were also preserved with 2% acid Lugol's solution and stored in the dark at 6°C until analysis with a FlowCam 8000 (Fluid Imaging Technologies) using a 100 µm flow cell, at ×10 magnification and 13 frames s^{-1}. FlowCam images were identified by the internal software, which calculates cell volumes using the factory-calibrated pixel size. Samples were categorized broadly into Bacillariophyceae, Dinophyceae, Cyanophyceae, and 2 size classes of unidentified plankton (<10 and >10 µm). Class Cyanophyceae was divided into coccoid and filamentous forms and the latter included Order Oscillatoriales, which were counted only by FlowCam. In addition, one specific genus of green algae, *Monoraphidium* spp., was distinguished. Sampling day (representing the starting community) and experiment Days 5, 19, and 33 were chosen for the community analyses. The same FlowCam images were also used to visualize the relative biovolume (%) of particles in different size fractions by classifying them into 11 different size groups based on their diameter (<5, 5–9, 10–19, 20–29, 30–39, 40–49, 50–59, 60–69, 70–79, 80–90, and >90 µm) on the sampling day (Start) and experiment Days 5, 19, 33, and 35.

Heterotrophic dinoflagellates and ciliates were enumerated by inverted light microscope (Leitz DM IRB, Leica) on Days 1, 5, 19, and 33 except for the coldest N-treated unit, where instead of Day 19, Days 15 and 22 were enumerated due to a missing sample. The abundance of diazotrophic cyanobacteria (*Aphanizomenon* sp., *Dolichospermum* spp., and *Nodularia spumigena*) was counted with a light microscope (Leica DMI 3000B) from samples taken at the start of the experiment and on Day 35. Using the appropriate stereometric formula, the biovolume and composition were determined according to HELCOM guidelines (HELCOM 2021).

2.5. Data analysis

The disappearance of DIP was treated as active uptake, and the uptake rate was calculated for each experimental unit by linear regression (DIP concentration vs. time in days). The DIP uptake rate for each experimental unit was calculated until the phosphate concentration reached the limit of concentration of reduced precision, which is 0.096 µmol l^{-1}. The value of the estimated slope of the linear regression line is considered the uptake rate, i.e. the concentration of consumed phosphate (µM) per day. Similarly, temperature effects on phosphate uptake rate were assessed by linear regression analysis, with the slope describing the direction and magnitude of change. The DIN:DIP uptake ratio was calculated as an average for the 3 N-treated units based on the decrease in the known concentration of added NO_3^- in relation to the decline in the phosphate concentration during experiment Days 1–12. Statistical differences in the stoichiometry of particulate organic matter between the control and N-treatment were tested using the nonparametric pairwise Mann-Whitney *U*-test, and results were considered significant at $p < 0.05$. In addition, we performed multivariate analyses of the abundances of the 4 plankton populations measured by flow cytometry (heterotrophic bacteria, *Synechococcus*-like picocyanobacteria, picoeukaryotes, and nanophytoplankton) and 3 environmental variables (temperature, NO_3^- concentration, and experiment day) using non-metric multidimensional scaling (NMDS) with the 'metaMDS' and 'envfit' functions in the R package 'vegan' (Oksanen et al. 2022). The 'envfit' function was used to fit environmental vec-

tors onto the NMDS ordination plot to determine how much of the variability in the ordination scores of the first (NMDS1) and second (NMDS2) axes of the NMDS are explained by temperature, NO_3^- concentration, and experiment day. The significance of the 3 fitted environmental vectors (p-value) is assessed by using permutation of environmental variables, and the goodness-of-fit statistics is the squared correlation coefficient (r^2). All statistical analyses were performed using R v.4.2.2 (R Core Team 2022), and plots were created using the package 'ggplot2' (Wickham 2016) except for the NMDS plots, for which the base R was used.

3. RESULTS

3.1. Inorganic nutrient uptake

The consumption rate of phosphate was 2.3–3.2 times faster in the N-treatment compared to the control. On the last day of the experiment, phosphate concentration was above the detection limit only in the coldest control unit (0.12 µmol l^{-1}; Fig. 1A). The equations of the linear regression between phosphate concentrations and day of the experiment in different treatments are presented in Table S1 in the Supplement at www.int-res.com/articles/suppl/m718 p023_supp.pdf. Higher experimental temperature increased the phosphate uptake rate in the control units ($r^2 = 0.99$, $p = 0.022$), while the uptake rate in N-treated units was relatively constant across the temperature gradient (0.037–0.039 µM d^{-1}) (Fig. 1B).

The NO_3^- added after each sampling in the N-treatment was close to or below the detection limit during the following sampling. The average NO_3^- concentration was 0.06 µmol l^{-1}, with no apparent difference between the treatments throughout the experiment (data not shown). Ammonium concentrations were low throughout the experiment in all units (<0.19 µmol l^{-1}; data not shown). The DIN:DIP uptake ratio calculated for the N-treated units was 4.6, and thus well below the Redfield ratio (16).

3.2. Dynamics of dissolved and particulate organic nutrients

The variability of DOC and DON concentrations did not show treatment effects (Fig. 2A,B). The DOP concentration in N-treated units increased until DIP was depleted on Day 15 (Fig. 2C). A steep decrease in DOP concentrations occurred between Days 15 and 19 in all N-treated units, with the highest drop from 0.61 to 0.34 µmol l^{-1} at 13°C, meaning that all DOP that had accumulated during the first 15 d of the

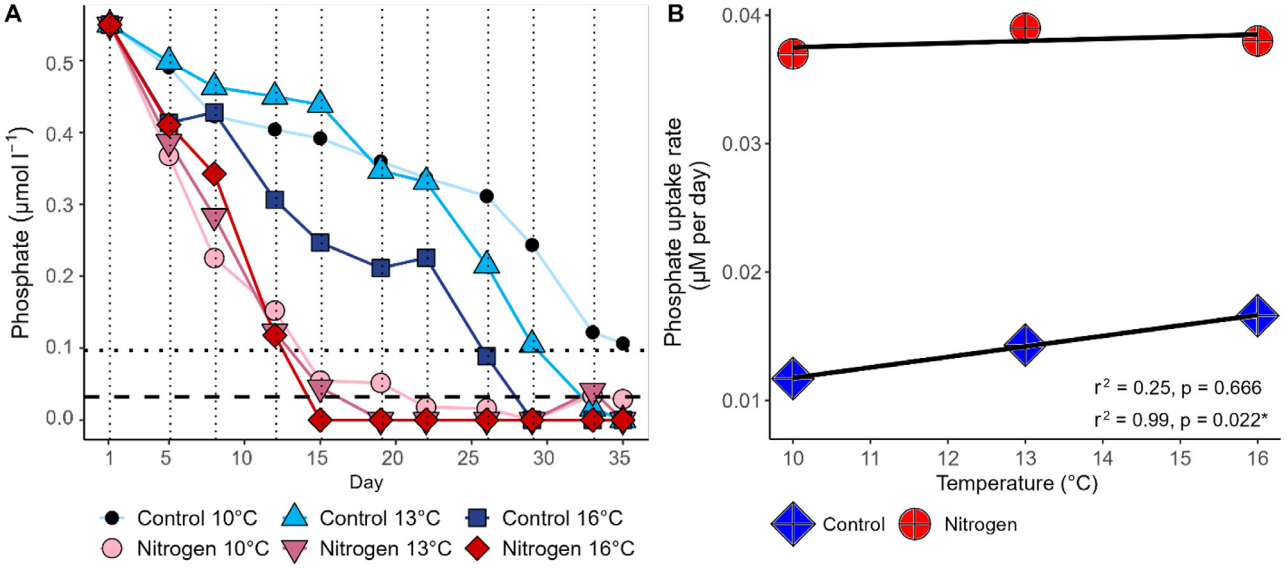

Fig. 1. (A) Development of phosphate concentration over time. Vertical lines: nitrate addition after sampling in the nitrogen-amended units (red symbols); dotted horizontal line: concentration with reduced precision; dashed horizontal line: analytical detection limit. (B) Phosphate uptake rates as a function of temperature in control and N-treated units. The uptake rates were calculated until the phosphate concentration reached the limit of concentration of reduced precision (dotted line in A), which were Days 1–12 for the nitrogen-amended units, Days 1–26 for control at 16°C, Days 1–29 for control at 13°C, and Days 1–35 for control at 10°C

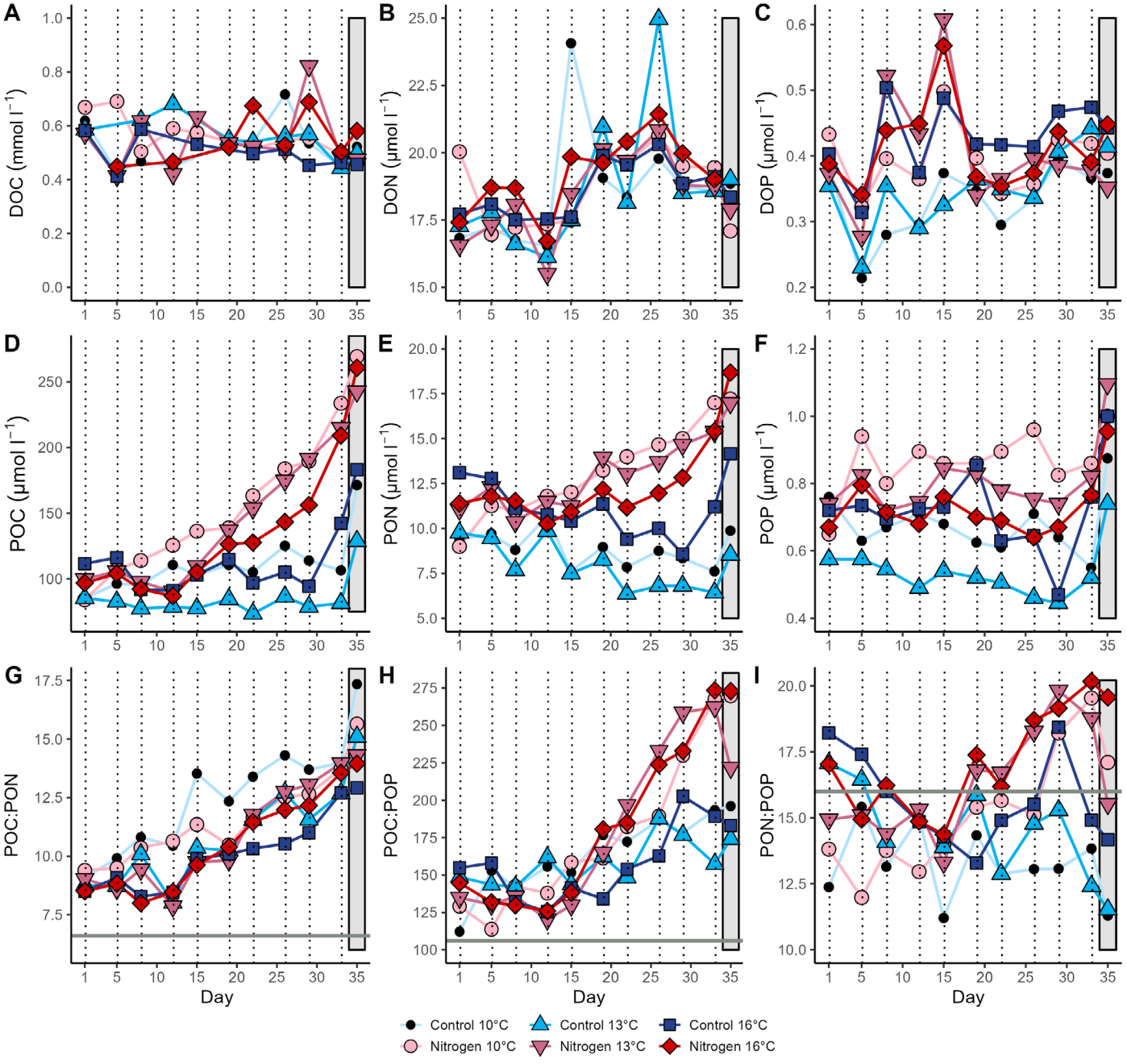

Fig. 2. Development of concentrations of (A) dissolved organic carbon (DOC), (B) dissolved organic nitrogen (DON), (C) dissolved organic phosphorus (DOP), (D) particulate organic carbon (POC), (E) particulate organic nitrogen (PON), (F) particulate organic phosphorus (POP), and (G,H,I) elemental ratios of particulate organic nutrients over time. Vertical lines: nitrate addition after sampling in the nitrogen-amended units (red symbols); grey boxes: the last sampling when sedimented material was included; horizontal lines in (G,H,I): molar Redfield ratios

experiment was degraded. The development of DOP concentration in the warmest control unit differed from the 2 colder units and resembled the development of the N-treated ones. After the decrease on Day 19, low concentrations of DOP were released again in all units.

Nitrogen addition resulted in a pronounced and constant build-up of POC and PON in all 3 temperatures from Day 12 onwards (Fig. 2D,E), thus closely following the start of the increase in chl *a* concentrations (Fig. S1). The POC concentrations of the N-treated units more than doubled between Days 1 and

33 (from 93.5 ± 8.4 to 219.1 ± 10.7 µmol l^{-1}, on average). By contrast, the concentration of control units was relatively constant (between 93.9 ± 12.5 and 110.0 ± 25.0 µmol l^{-1}, on average) until the last sampling on Day 35. When all the sedimented material was included on Day 35, POC concentrations were, on average, 257 ± 12.4 and 161.0 ± 23.6 µmol l^{-1} in the N-treated and control units, respectively. The PON concentration increased from ~10.5 to ~15.9 µmol l^{-1} in N-treatments and decreased from ~10.8 to ~8.4 µmol l^{-1} in the control treatments between Days 1 and 33. On Day 35, the PON concentration in the N-treatment was, on average, 17.6 ± 1.0 µmol l^{-1} and similar in all temperatures, while there was a more considerable variation in the control units with ~10.9 ± 2.4 µmol l^{-1}. During the regular sampling days, the POP concentration fluctuated within the range of 0.42–0.97 µmol l^{-1} with a slight increasing trend in the N-treated units and a decreasing trend in control (Fig. 2F). The POP concentration on Day 35 was 0.12–0.28 and 0.29–0.35 µmol l^{-1} higher in the control and N-treated units compared to the starting concentrations, respectively, meaning that depending on the experimental conditions, between 22 and 64% of the excess phosphate (0.55 µmol l^{-1}) ended up in the POP pool.

The ratios of POC:PON and POC:POP were already much higher than Redfield stoichiometry (6.6 and 106, respectively) at the beginning of the experiment (Fig. 2G,H). The POC:POP and PON:POP ratios started to increase in the N-treated units on Day 15 as DIP became depleted in the warmest unit (16°C), and the concentrations at 10 and 13°C were low (0.055 and 0.045 µmol PO_4^{3-} l^{-1}, respectively; Fig. 1A). The POC:POP ratio also increased in the control units, which was attributed to the relatively stable POC and decreasing POP concentrations over time. N-addition did not affect the POC:PON ratios but resulted in, on average, 1.5- and 1.4-fold higher POC:POP and PON:POP ratios during the last regular sampling on Day 33, respectively. On Day 35, the POC:POP ratio exceeded the Redfield value by a factor of 2.4 in the N-treated units and 1.7 in the control ones. At the onset of the experiment, PON:POP ratios (12.3–18.2) ranged around the Redfield value of 16 but increased slightly above the Redfield ratio in the N-treatment during the second half of the experiment (Fig. 2I). The PON:POP ratios in the control units were generally slightly below the Redfield ratio throughout the experiment, reflecting the low DIN:DIP ratio.

Changes in the relative contributions of different forms of the total phosphorus pool showed a higher increase of POP (between 20 and 31%) compared to DOP (between 0 and 7%) between Days 1 and 35 (Fig. 3). The contribution of different size fractions to the total biovolume measured by the FlowCam showed an increasing trend of larger sized particles over time in all experimental units (Fig. S2). This trend was most pronounced at 16°C where the contribution of particles >50 µm to the total biovolume more than doubled from the starting contribution of 23.0% to 57.5% (Control) and 50.7% (N-treatment) on the last day of the experiment (Fig. S2).

3.3. Development of plankton community

The flow cytometry data and the NMDS analyses indicated that there was a significant temporal development ($r^2 = 0.58$, $p = 0.001$) in the abundances of the 4 plankton populations measured by flow cytometry (Fig. S3A,B). The small-sized plankton groups (heterotrophic bacteria, *Synechococcus*-like picocyanobacteria, and picoeukaryotes) increased during the first half of the experiment and then declined (Fig. 4A–C), whereas nanophytoplankton seemed to favor nitrogen and was the only group that peaked after phosphate depletion during the second half of the experiment (Fig. 4D). Nanophytoplankton abundance was lower in the control units compared to the N-treated ones throughout the experiment, which was also indicated by the NMDS analyses that showed a negative correlation between NO_3^- concentration and the NMDS2 ordination score, suggesting that the higher NO_3^- concentration led to a relative increase in nanophytoplankton abundance ($r^2 = 0.12$, $p = 0.023$). However, the data was not evenly distributed along the NO_3^- axis but rather gathered into 2 groups (control and N-treatment) as illustrated in Fig. S3C, which decreases the goodness of the fit. Abundances of both heterotrophic bacteria and *Synechococcus*-like picocyanobacteria were highest in the warmest control treatment unit. However, according to the NMDS analyses, high concentration of NO_3^- was associated with a reduction only in the picocyanobacterial abundance, and temperature had no significant effect on the plankton community measured by flow cytometry ($r^2 = 0.04$, $p = 0.273$).

Dinoflagellates initially dominated the microplankton community, with a contribution of 43.6% of the total biovolume (Fig. 5). The relative abundance of dinoflagellates declined in all treatments after Day 5. By contrast, the relative abundance of diatoms was

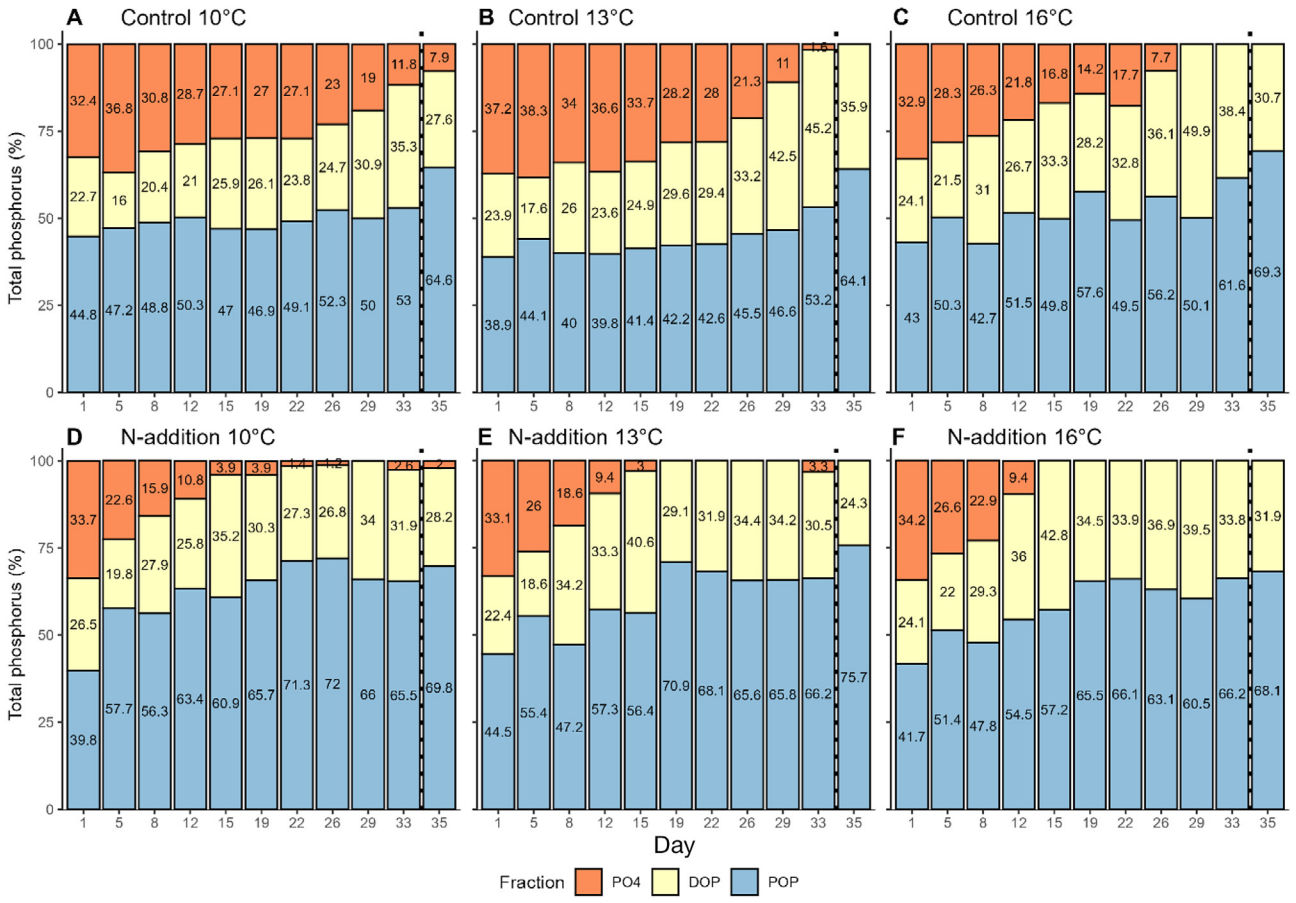

Fig. 3. Development of relative contributions of the different components (phosphate [PO_4^{3-}], dissolved organic phosphorus [DOP], and particulate organic phosphorus [POP]) to the total phosphorus pool during the experiment. Vertical dotted lines illustrate the different sampling technique that was used on Day 35

low at the beginning (9.2%), but increased until the middle of the experiment, after which it decreased in all units except those at 10°C. The depletion of DSi did not follow the development of chl *a* concentration (Fig. S1). Diatoms became dominated by the small-cell genera *Skeletonema* spp. and *Chaetoceros* spp. over time, which is consistent with the decreasing trend in the chl *a*:BSi ratio in all units (Fig. S1). The latter became especially abundant in the coldest N-treatment at the end of the experiment. Besides these taxonomic groups, *Monoraphidium* spp. became abundant (>60% of total biovolume) at the end of the experiment in the 2 warmest N-treated units, while their relative abundance in the control treatment remained low throughout the experiment (<8%). The relative abundance of organisms in the unidentified <10 µm increased over time in the control treatments, where it also seemed to increase with temperature (Fig. 5).

The biovolume of microscopically counted diazotrophic cyanobacteria was initially low (<0.5% of the total biovolume) and dominated by *Aphanizomenon* sp. (data not shown). On the last day of the experiment, *Aphanizomenon* sp. dominated the cyanobacteria biovolume at 10°C (0.026 $mm^3\ l^{-1}$) and 13°C (0.022 $mm^3\ l^{-1}$; Fig. 6), which corresponded to less than 3% of the total biovolume. *Dolichospermum* spp. occurred in the control units at 13 and 16°C, but their contribution to the total cyanobacteria biovolume was low; at the highest, 0.001 $mm^3\ l^{-1}$ in the control unit at 13°C (Fig. 6). *Nodularia spumigena* was not detected at the start. Still, its biovolume on the last sampling day ranged between 0.004 $mm^3\ l^{-1}$ in the N-treatment at 10°C and 0.033 $mm^3\ l^{-1}$ in the control unit at 16°C (Fig. 6), corresponding to 0.27 and 2.76% of the total biovolume, respectively.

Heterotrophic dinoflagellates were most abundant at the beginning but declined towards the end of the experiment in all units (Fig. S4). By contrast, the abundance of ciliates increased slightly over time, and the highest abundance was measured in the warmest N-treated unit (Fig. S4).

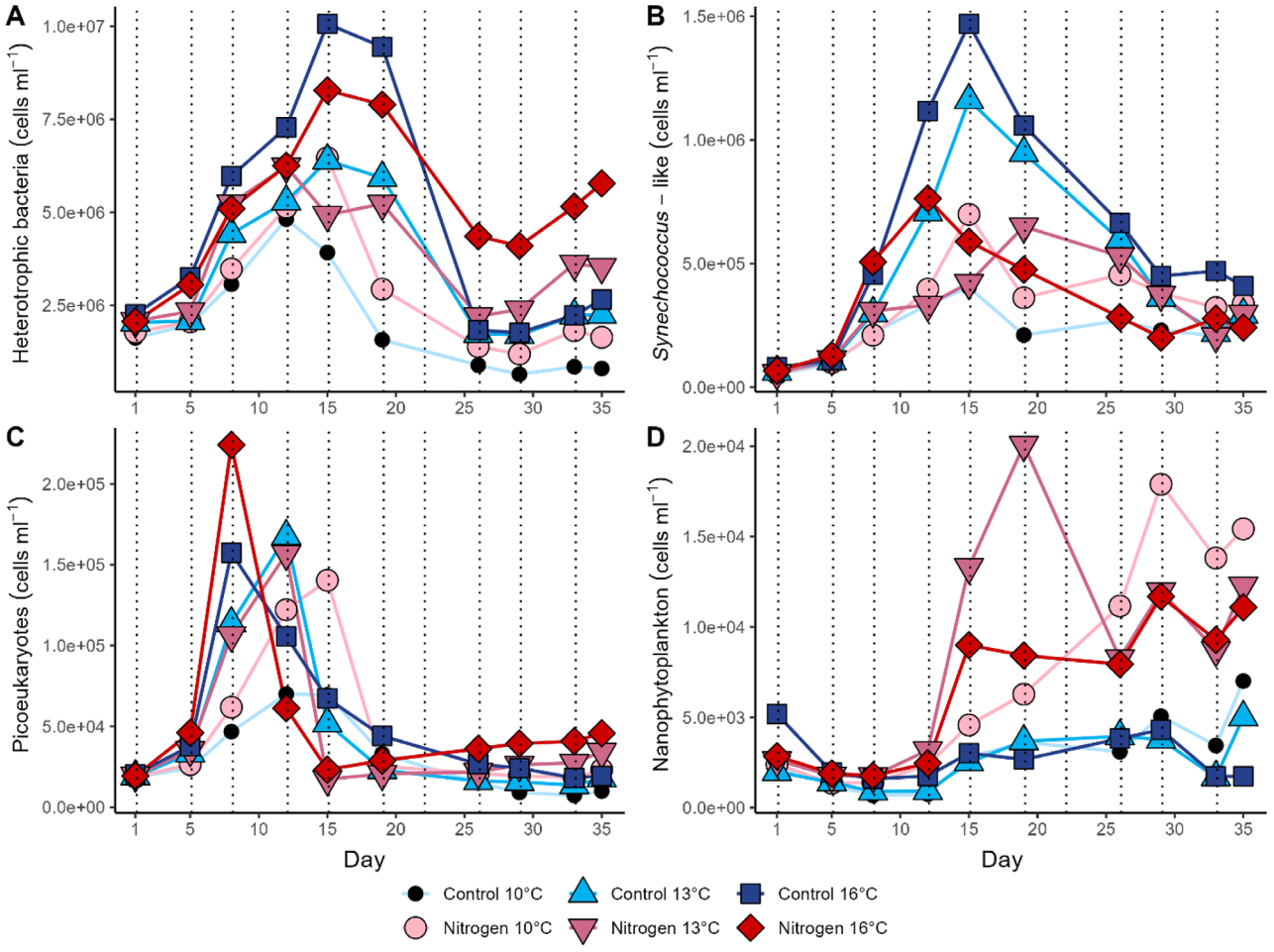

Fig. 4. Development of the abundance of communities measured by flow cytometry over time: (A) heterotrophic bacteria, (B) *Synechococcus*-like cyanobacteria, (C) picoeukaryotes, and (D) nanophytoplankton. Vertical lines illustrate nitrate addition after sampling in the nitrogen-amended units (red symbols)

4. DISCUSSION

4.1. Phosphate consumption and the DIN:DIP uptake ratio

We observed low DIN concentrations throughout the experiment, even in the N-amended units, indicating that the DIN added after each sampling was entirely consumed before the next addition. In the presence of a nitrogen supply, which in this study simulated the frequently occurring mixing events during the post-spring-bloom season (Spilling 2007), the DIN:DIP uptake ratio deviated from the molar Redfield ratio (16) and demonstrates the potential of luxury uptake and storage of phosphate relative to nitrogen. Although DIN-addition enhanced phosphate uptake rates up to 3-fold compared to the control, residual phosphate was depleted (<0.05 µmol l^{-1}) within 33 d, even in the 2 warmest control units, regardless of severe nitrogen depletion.

The community in the control units consumed the excess phosphate at higher rates than the 0.004–0.007 µM d^{-1} estimated by Lips & Lips (2017), which could be due to the stable growth conditions we used compared with the natural environment. Nausch et al. (2018) reported DIP uptake rates between 0.02 and 0.06 µM d^{-1} in our study area (the Tvärminne Archipelago) during June–July that are comparable to the DIP uptake rates (~0.04 µM d^{-1}) in the N-treated units in our study.

Elevated seawater temperatures are assumed to enhance nutrient uptake by altering the rates of cellular growth and metabolic activity of the plankton community (Hoppe et al. 2012, Boscolo-Galazzo et al. 2018). The effect of temperature on the phosphate uptake rate was significant only in the control units,

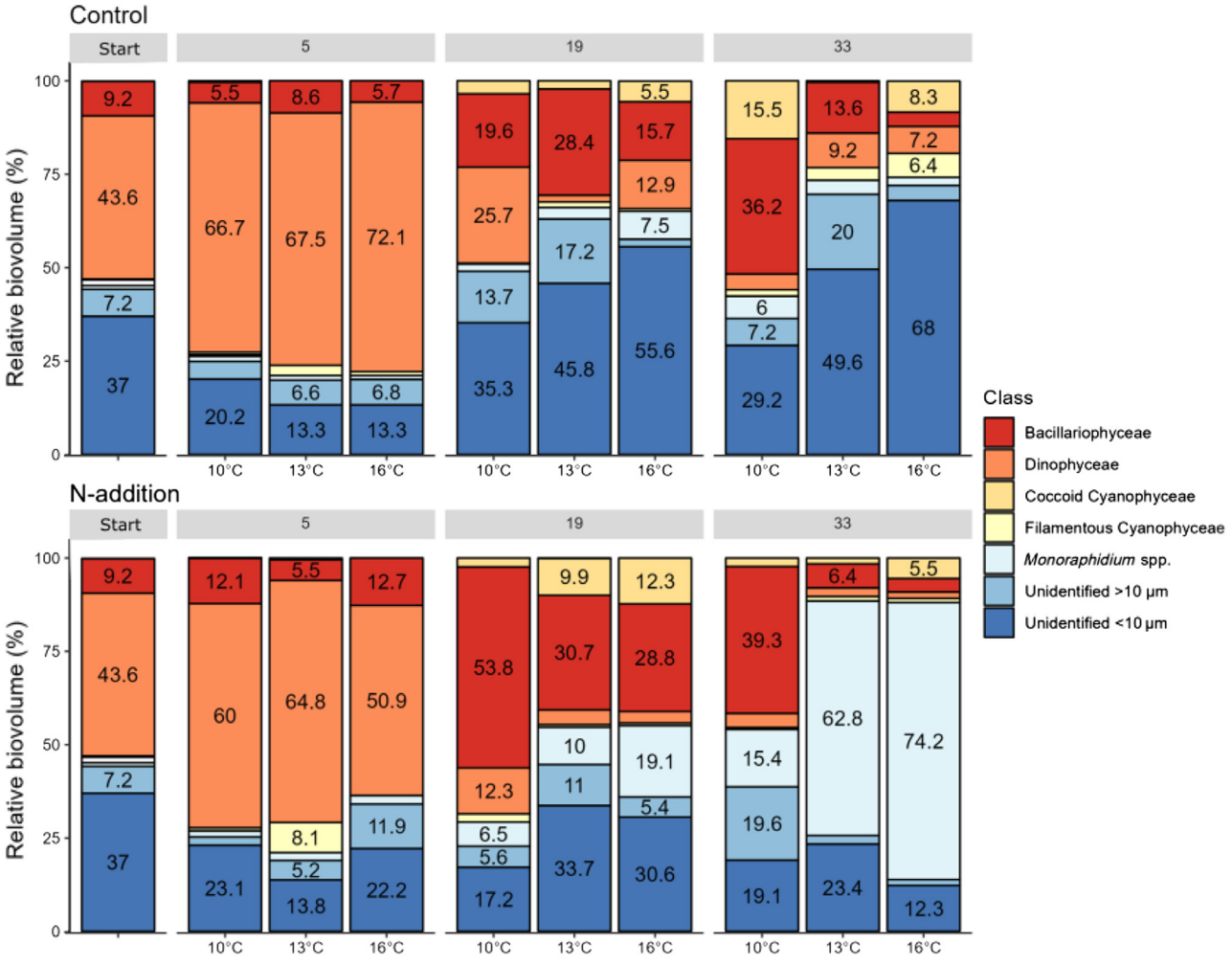

Fig. 5. Relative biovolume (%) of different functional groups measured with FlowCam at the start and the development of the community on experiment Days 5, 19, and 33. Values >5% are shown in the graph

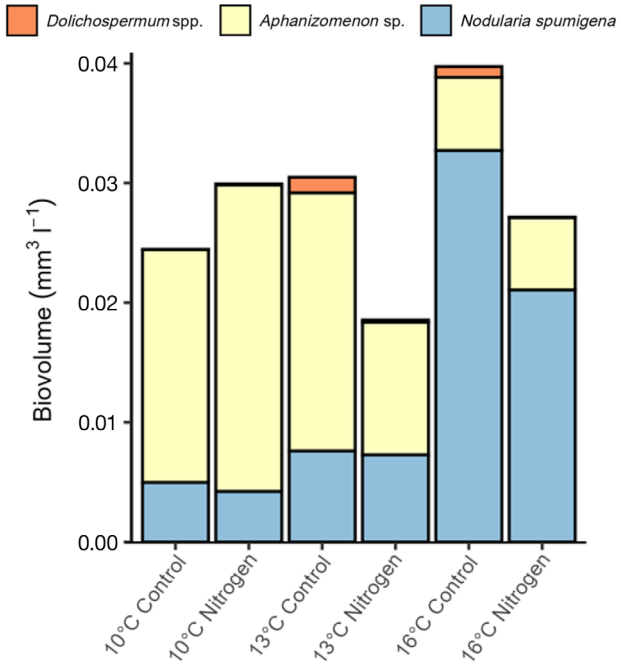

Fig. 6. Biovolumes of *Dolichospermum* spp., *Aphanizomenon* sp., and *Nodularia spumigena* on the last sampling day (Day 35)

which could result from increasing bacterial activity and remineralization of nitrogen with temperature. It is also possible that N_2-fixation by the diazotrophic cyanobacteria, which were most abundant in the highest experimental temperature and least abundant in the coldest control treatment on the last day of the experiment (Fig. 6), provided nitrogen for phosphate uptake in the control units. Temperature dependency of diazotrophic cyanobacteria is not possible to prove statistically based on our data, but our findings correspond to the general conception that *Nodularia spumigena* and *Dolichospermum* spp. have generally higher optimal growth temperature than other co-occurring autotrophs (Munkes et al. 2021).

4.2. Relation between excess phosphate and plankton community

Our results show that small organisms (<10 µm in this case) are important contributors to the depletion of DIP under nitrogen limitation, whereas larger nanophytoplankton require additional nitrogen sources to utilize the excess phosphate. Nausch et al. (2018) demonstrated that organisms in the size fraction of <3 µm were responsible for 71.5% of the DIP uptake on average in our study area. Experimental and theoretical evidence indicates that nutrient-limited conditions typically favor small cells with large surface-to-volume ratios and low minimum cellular metabolic requirements (Løvdal et al. 2007, Peter & Sommer 2013, Spilling et al. 2022). Heterotrophic bacteria are superior competitors for phosphate in the presence of external organic carbon sources (Drakare 2002, Joint et al. 2002). Their high metabolic rate and short generation times enable a relatively higher contribution to organic matter transformations and energy flow compared to larger organisms (Fenchel et al. 2012). The contribution of the abundant bacterial community (up to 1.0×10^7 cells ml^{-1}) to the excess phosphate uptake was probably crucial during the first half of the experiment when the substrate supply was sufficient. Likewise, the peaks in the abundances of picoeukaryotes and picocyanobacteria under severe nitrogen limitation during the first half of the experiment in the control units exemplify their ability to utilize excess phosphate by taking up recycled nitrogen at low concentrations.

In the control units, the fraction of <10 µm obtained by the FlowCam measurements dominated the community during the second phase of the experiment. In nature, this size fraction consists of a diverse community of bacteria, algae, and small protists. Our FlowCam measurements, however, do not account for bacteria and therefore the fraction <10 µm mostly consisted of small eukaryotes. In the control units, none of the groups measured by flow cytometry showed high abundances after the peaks during the first half of the experiment. Yet the phosphate concentration continued to decrease over time. This inconsistency raises the question of what took up the phosphate during the latter part of the experiment, and this question cannot be answered unequivocally based on our results. Marine particle aggregates often harbor dense bacterial communities (Simon et al. 2002). The size distribution and concentration of marine particles affect the rate at which bacteria encounter them (Kiørboe et al. 2002). With an increasing amount of large detritus-like material found in our study, it is possible that particle-associated bacteria, which we were not able to detect with flow cytometry, increased in the control units and consumed part of the available phosphate.

The simultaneous decrease of pico-sized fraction and the increase of nanophytoplankton during the second half of the experiment could have been caused by higher grazing pressure on the pico-sized community compared to the larger size fractions. This is supported by our NMDS results which indicated that temporal development was the main driver of small sized plankton in our experiment. Alternatively, larger organisms might use intracellular phosphorus reserves or DOP during DIP depletion. The latter explanation is supported by the decreasing DOP concentrations in the N-amended units and the warmest control unit during the second half of the experiment. However, heterotrophic bacteria also consume the bioavailable fraction of DOP (Nausch & Nausch 2007, Sisma-Ventura & Rahav 2019) and often dominate its uptake at the expense of phytoplankton when phosphorus is the limiting nutrient (Løvdal et al. 2007, Nausch et al. 2018), which points to the grazing explanation. In our study, ciliates were the top grazers due to 50 µm prescreening that excluded larger individuals of microzooplankton and mesozooplankton. Lips et al. (2014) and Lips & Lips (2017) suggested that the mixotrophic ciliate *Mesodinium rubrum* was responsible for depleting the excess phosphate by exploiting DIN in deeper, nutrient-rich layers. In general, *M. rubrum* is known for its high nutrient uptake rate and competitiveness under nutrient-limiting conditions (Lagus et al. 2004). Still, in our study, this species was not particularly abundant, and the heterotrophic genus *Euplotes* spp., which is known to feed on bacteria (Turley et al. 1986), became the dominant ciliate over time and was likely better adapted to the enclosure conditions that precluded any vertical migration.

The nano-size green algae *Monoraphidium* spp. took advantage of the added nitrogen and became the dominant autotroph over time at 13 and 16°C in the N-treatment. Many species of the genus *Monoraphidium* spp. favor eutrophic conditions in our study region (Kuosa 1988), and *M. contortum* was considered inedible in previous mesocosm studies in the Baltic Sea (Andersson et al. 2006), which explains their dominance in the N-treatment at the end of our experiment. Interestingly, the abundance of small diatoms also increased under nitrogen supply in our study after their low presence at the beginning of the experiment. In particular, *Chaetoceros* spp., which has a high affinity to low-nutrient concentra-

tions (Turpin & Harrison 1979), increased towards the end of the experiment. This trait, together with a high growth rate (Reynolds 2006, Spilling & Markager 2008) and adaptation to cooler temperatures (Finkel et al. 2010), likely explains their high relative abundance in the coldest treatments both in the control and N-amended units.

Filamentous N_2-fixing cyanobacteria are known to take up excess phosphate and polymerize it in the form of polyphosphate granules for intracellular storage without immediate growth (Allen 1984, Larsson et al. 2001, Benzerara et al. 2014). In general, the availability of excess phosphate did not cause a high growth of the 3 bloom-forming filamentous cyanobacteria genera in our study. The biovolumes of *Aphanizomenon* sp. and *Dolichospermum* spp. were well below the mean summer biovolumes summarized by Olofsson et al. (2020) in all treatments. However, *N. spumigena* reached biovolumes close to the mean summer values in the Gulf of Finland (0.045 $mm^3\ l^{-1}$; Olofsson et al. 2020) in the control treatment at 16°C in which the low DIN:DIP ratio, availability of DOP during DIP depletion, and sufficient temperature likely favored its growth. This also demonstrates the potential of a small pelagic seeding population of *N. spumigena* to reach bloom concentrations under favorable conditions (Wasmund 2017). Despite the potential to grow close to summer concentrations, the biovolume of the 3 main bloom-forming diazotrophic cyanobacteria accounted for, at the most, only 5.3% of the total biovolume at the end of the experiment and, therefore, only marginally affected the excess phosphate uptake. Based on literature values of a biovolume to carbon conversion factor of 0.56 pg C μm^{-3} for bacteria (Bratbak 1985) and a C:P ratio of 40, which is the low value reported for the common Baltic Sea cyanobacteria *Aphanizomenon* sp. (Walve & Larsson 2007), we calculated that the maximum phosphorus content in the filamentous cyanobacteria found in our experimental units on the last day of our study was <3% of the available phosphate at the start of the experiment. Altogether, these results suggest that the main phosphorus sources for the cyanobacterial blooms in summer come not from direct uptake, but likely from deeper water layers through e.g. vertical migration, mixing, or upwelling events (Nausch et al. 2004, 2012, Wasmund et al. 2005, Walve & Larsson 2007). Studies that utilize imaging tools to investigate phosphorus incorporation and distribution at the cellular level (Braun et al. 2018) or ^{32}P-labeled phosphate to evaluate phosphate uptake kinetics (such as in Aubriot 2019) are needed to more accurately follow the phosphate fluxes into organisms and to further clarify the contribution of filamentous cyanobacteria to the uptake of excess phosphate.

4.3. Phosphorus turnover and flux

Nitrogen addition resulted in significantly higher POC:POP and PON:POP ratios than non-amended units. This suggests that inorganic nutrient concentration was the most critical factor in determining the elemental stoichiometry of organic matter and corroborates a recent study in the Baltic Sea (Cabrerizo et al. 2021). The POC:PON and POC:POP ratios of the present study were constantly higher than the Redfield values of 6.6 and 106, respectively. This finding is in line with several other observations and model simulations in the Baltic Sea (Schneider et al. 2003, Wasmund et al. 2005, Kreus et al. 2015, Lipsewers et al. 2020) and suggests inorganic phosphorus and nitrogen (even in the N-amended units) limitation of the plankton community and continued carbon fixation by phytoplankton after inorganic nutrients were depleted. The POC:POP ratio increased in response to decreasing phosphate availability in all units, but the high variability (C:P ratio between 125.0 and 272.9) below the concentration of 0.097 µmol DIP l^{-1} indicates decoupling between nutrient uptake and phytoplankton growth, which demonstrates stoichiometric flexibility of the post-spring-bloom plankton community.

In theory, excessive carbon fixation results in the formation of nutrient-poor particulate matter, making it more resistant to microbial remineralization and potentially enhancing the export flux of organic matter due to preferred remineralization of nitrogen and phosphorus than organic carbon in particles (Boyd & Trull 2007). Overconsumption of carbon relative to inorganic nitrogen and the resulting increase in the POC:PON ratio have been associated with the formation of transparent exopolymer particles (TEP) that can coagulate into larger particle aggregates and thus contribute to organic matter export (Engel et al. 2002). In our study, TEP was not measured, but diatoms, such as *Chaetoceros* spp., that are known to produce precursors of TEP in the water (Passow 2002) were present and relatively abundant.

The DOP concentrations measured in this study (0.21–0.61 µmol l^{-1}) were close to the values measured in the central Baltic Sea (0.2–0.52 µmol l^{-1}) but lower than the maximum concentration reported in the coastal areas of this region (0.98 µmol l^{-1}; Hoikkala et al. 2015). During the first half of the experiment, part of the assimilated phosphate seemed to accumulate as

bioavailable DOP that was quickly consumed at the beginning of the phosphate-limited second half of the experiment but slightly increased again towards the end of the study, resulting in an overall increase of, on average, 0.002 µmol DOP l^{-1} in the N-treatment and 0.03 µmol DOP l^{-1} in the control throughout the experiment (Fig. 2C). The model results of Kreus et al. (2015) suggested that labile DOP remaining in the surface water after the spring bloom could fuel the growth of cyanobacteria. Our results, however, suggest that only a small part of the excess phosphate would end up in the DOP pool and, in addition, a large fraction of the DOP (~0.21–0.34 µmol l^{-1}) was probably refractory; this amount is higher than concentrations measured in natural conditions in the Gulf of Finland but consistent with findings that major part of the DOP pool in the Baltic Sea is refractory (~0.1–0.2 µmol refractory DOP l^{-1}; Nausch & Nausch 2011).

The decline of phosphate concentration was not reflected as an increase in the POP pool during our regular samplings between Days 1 and 33. However, when the sedimented material sampled on the last day of the experiment (Day 35) was included in the total phosphorus budget, an increase of POP between the beginning and the end of the study of, on average, 0.19 µmol l^{-1} in the control and 0.32 µmol l^{-1} in the N-treatment was observed (Fig. 2F). This observed higher increase in the concentration of POP compared to DOP would support the theory that a larger part of the assimilated phosphate would settle out from the surface layer after the spring bloom under natural conditions (Nausch et al. 2004). In addition, FlowCam images revealed an increasing amount of large detritus-like material and aggregated algae that would most likely sink out from the euphotic zone (Fig. S2). Although size is an important factor influencing particle sinking speed, more accurate estimates of the sinking potential and flux of POM would require measurements of remineralization processes and particle characteristics, such as chemical composition, porosity, and mineral ballasting.

Part (2–21 %) of the starting total phosphorus concentration was unaccounted for at the end of the experiment. This unaccountable part of the total phosphorus pool might have ended up in the size fraction between the filtrates of DOP and POP (0.2–0.8 µm). Another possibility is that it was contained in the biomass that adhered to the walls of the experimental units, which did not loosen even with vigorous shaking on the final day. A combination of both possibilities is likely the reason for the missing phosphorus in our phosphorus budget.

5. CONCLUSIONS

The results of this study demonstrate the ability of the post-spring-bloom community to deplete excess phosphate under severe nitrogen depletion and suggest that other sources of phosphate are likely needed to support the extensive blooms of filamentous cyanobacteria during late summer in the northern Baltic Sea. More accurate methods, such as imaging tools and isotope techniques in different size fractions of the plankton community, should be used in future studies to more accurately follow the flux of phosphate into cells. Our study provides important empirical data regarding the uptake ratio of DIN and DIP in the northern Baltic during the post-spring-bloom season, which is important for modeling studies that intend to forecast future cyanobacterial blooms in the Baltic Sea. The results indicate that assimilated excess phosphate has the potential to sink down to the benthic system as POP via aggregates formed after the excess phosphate has been utilized in the surface layer. Larger mesocosm studies are required to reduce the bottle effect and improve the estimates of the different components of the total phosphorus pool during the post-spring-bloom phase.

Acknowledgements. We thank Jostein Solbakken for assistance in field sampling, Mervi Sjöblom and Jaana Koistinen for inorganic and organic nutrient analyses and the staff at the Tvärminne Zoological Station during the experiment. We also thank Harri Kuosa and Heidi Hällfors for their help in phytoplankton identification and Harri Kuosa for support in manuscript preparation. We extend our thanks to Riina Klais-Peets for help with the NMDS statistics. The study utilized the Finnish Environment Institute marine research infrastructure as a part of the national Finnish Marine Research Infrastructure (FINMARI) consortium. This study was funded by the Walter and Andrée de Nottbeck Foundation and Koneen Säätiö.

LITERATURE CITED

Alegria Zufia J, Farnelid H, Legrand C (2021) Seasonality of coastal picophytoplankton growth, nutrient limitation and biomass contribution. Front Microbiol 12:786590

Allen MM (1984) Cyanobacterial cell inclusions. Annu Rev Microbiol 38:1–25

Andersson A, Samuelsson K, Haecky P, Albertsson J (2006) Changes in the pelagic microbial food web due to artificial eutrophication. Aquat Ecol 40:299–313

Aubriot L (2019) Nitrogen availability facilitates phosphorus acquisition by bloom-forming cyanobacteria. FEMS Microbiol Ecol 95:fiy229

Benzerara K, Skouri-Panet F, Li J, Férard C and others (2014) Intracellular Ca-carbonate biomineralization is widespread in cyanobacteria. Proc Natl Acad Sci USA 111:10933–10938

Boscolo-Galazzo F, Crichton KA, Barker S, Pearson PN (2018) Temperature dependency of metabolic rates in the upper ocean: A positive feedback to global climate change? Global Planet Change 170:201–212

Boyd P, Trull T (2007) Understanding the export of biogenic particles in oceanic waters: Is there consensus? Prog Oceanogr 72:276–312

Bratbak G (1985) Bacterial biovolume and biomass estimations. Appl Environ Microbiol 49:1488–1493

Braun PD, Schulz-Vogt HN, Vogts A, Nausch M (2018) Differences in the accumulation of phosphorus between vegetative cells and heterocysts in the cyanobacterium *Nodularia spumigena.* Sci Rep 8:5651

Cabrerizo MJ, Marañón E, Fernández-Gonzáles C, Alonso-Núñez A, Larsson H, Aranguren-Gassis M (2021) Temperature fluctuation attenuates the effect of warming in estuarine microbial plankton communities. Front Mar Sci 8:656282

Conley DJ (2012) Save the Baltic Sea. Nature 486:463–464

Conley DJ, Humborg C, Rahm L, Savchuk OP, Wulff F (2002) Hypoxia in the Baltic Sea and basin-scale changes in phosphorus biogeochemistry. Environ Sci Technol 36: 5315–5320

Drakare S (2002) Competition between picoplanktonic cyanobacteria and heterotrophic bacteria along crossed gradients of glucose and phosphate. Microb Ecol 44: 327–335

Engel A, Goldthwait S, Passow U, Alldredge A (2002) Temporal decoupling of carbon and nitrogen dynamics in a mesocosm diatom bloom. Limnol Oceanogr 47:753–761

Fenchel T, King GM, Blackburn TH (2012) Bacterial biogeochemistry: the ecophysiology of mineral cycling, 3rd edn. Academic Press, Amsterdam

Finkel ZV, Beardall J, Flynn K, Qui GGA, Rees TAV, Raven JA (2010) Phytoplankton in a changing world: cell size and elemental stoichiometry. J Plankton Res 32:119–137

Gasol JM, Del Giorgio PA (2000) Using flow cytometry for counting natural planktonic bacteria and understanding the structure of planktonic bacterial communities. Sci Mar 64:197–224

Grasshoff K, Ehrhardt M, Kremling K (eds) (1999) Methods of seawater analysis, 3rd edn. Wiley-VCH, Weinheim

Heiskanen AS (1998) Factors governing sedimentation and pelagic nutrient cycles in the northern Baltic Sea. Monogr Boreal Env Res 8:1–80

HELCOM (Helsinki Commission) (2021) Guidelines for monitoring of phytoplankton species composition, abundance and biomass. Baltic Marine Environment Protection Commission, Helsinki

Hoikkala L, Kortelainen P, Soinne H, Kuosa H (2015) Dissolved organic matter in the Baltic Sea. J Mar Syst 142: 47–61

Hoppe HG, Giesenhagen HC, Koppe R, Hansen HP, Gocke K (2012) Impact of change in climate and policy from 1988 to 2007 on environmental and microbial variables at the time series station Boknis Eck, Baltic Sea. Biogeosciences Discuss 9:18655–18706

Joint I, Henriksen P, Fonnes GA, Bourne D, Thingstad TF, Reimann B (2002) Competition for inorganic nutrients between phytoplankton and bacterioplankton in nutrient manipulated mesocosms. Aquat Microb Ecol 29:145–159

Karlson AML, Duberg J, Motwani NH, Hogfors H and others (2015) Nitrogen fixation by cyanobacteria stimulates production in Baltic food webs. Ambio 44(Suppl 3): S413–S426

Kiørboe T, Grossart HP, Ploug H, Tang K (2002) Mechanisms and rates of colonisation of sinking aggregates. Appl Environ Microbiol 68:3996–4006

Kirchman DL (1994) The uptake of inorganic nutrients by heterotrophic bacteria. Microb Ecol 28:255–271

Koistinen J, Sjöblom M, Spilling K (2017) Determining inorganic and organic phosphorus. In: Spilling K (ed) Biofuels from algae. Humana Press, New York, NY, p 87–94

Koistinen J, Sjöblom M, Spilling K (2018) Determining dissolved and biogenic silica. In: Spilling K (ed) Methods in molecular biology. Humana Press, New York, NY, p 95–102

Kreus M, Schartau M, Engel A, Nausch M, Voss M (2015) Variation in the elemental ratio of organic matter in the central Baltic Sea: Part I—linking primary production to remineralization. Cont Shelf Res 100:25–45

Kuosa H (1988) Observations on the taxonomy and ecology of *Monoraphidium* (Chlorophyceae, Chlorococcales) and *Koliella* (Chlorophyceae, Ulotrichales) species in Tvärminne Sea area, SW coast of Finland. Arch Protistenkd 135:45–53

Kuparinen J, Tuominen L (2001) Eutrophication and self-purification: counteractions forced by large-scale cycles and hydrodynamic processes. Ambio 30:190–194

Lagus A, Suomela J, Weithoff G, Heikkilä K, Helminen H, Sipura J (2004) Species-specific differences in phytoplankton responses to N and P enrichments and the N:P ratio in the Archipelago Sea, northern Baltic Sea. J Plankton Res 26:779–798

Larsson U, Hajdu S, Walve J, Elmgren R (2001) Baltic Sea nitrogen fixation estimated from the summer increase in upper mixed layer total nitrogen. Limnol Oceanogr 46: 811–820

Lehtoranta J, Savchuk OP, Elken J, Dahlbo K and others (2017) Atmospheric forcing controlling inter-annual nutrient dynamics in the open Gulf of Finland. J Mar Syst 171:4–20

Lignell R, Heiskanen AS, Kuosa H, Gundersen K, Kuuppo-Leinikki P, Pajuniemi R, Uitto A (1993) Fate of a phytoplankton spring bloom: sedimentation and carbon flow in the planktonic food web in the northern Baltic. Mar Ecol Prog Ser 94:239–252

Lips I, Lips U (2017) The importance of *Mesodinium rubrum* at post-spring bloom nutrient and phytoplankton dynamics in the vertically stratified Baltic Sea. Front Mar Sci 4:407

Lips I, Rünk N, Kikas V, Meerits A, Lips U (2014) High-resolution dynamics of the spring bloom in the Gulf of Finland of the Baltic Sea. J Mar Syst 129:135–149

Lipsewers T, Klais R, Camarena-Gómez MT, Spilling K (2020) Effects of different plankton communities and spring bloom phases on seston C:N:P:Si:chl *a* ratios in the Baltic Sea. Mar Ecol Prog Ser 644:15–31

Löptien U, Dietze H (2022) Ambiguous controls on simulated diazotrophs in the world oceans. Sci Rep 12:17784

Løvdal T, Tanaka T, Thingstad TF (2007) Algal–bacterial competition for phosphorus from dissolved DNA, ATP, and orthophosphate in a mesocosm experiment. Limnol Oceanogr 52:1407–1419

Moorthi SD, Schmitt JA, Ryabov A, Tsakalakis I and others (2016) Unifying ecological stoichiometry and metabolic theory to predict production and trophic transfer in a marine planktonic food web. Philos Trans R Soc Lond B Biol Sci 371:20150270

Munkes B, Löptien U, Dietze H (2021) Cyanobacteria blooms in the Baltic Sea: a review of models and facts. Biogeosciences 18:2347–2378

Murray CJ, Müller-Karulis B, Carstensen J, Conley DJ, Gustafsson BG, Andersen JH (2019) Past, present and future eutrophication status of the Baltic Sea. Front Mar Sci 6:2

Nausch M, Nausch G (2007) Bioavailable dissolved organic phosphorus and phosphorus use by heterotrophic bacteria. Aquat Biol 1:151–160

Nausch M, Nausch G (2011) Dissolved phosphorus in the Baltic Sea—occurrence and relevance. J Mar Syst 87: 37–46

Nausch M, Nausch G, Wasmund N (2004) Phosphorus dynamics during the transition from nitrogen to phosphate limitation in the central Baltic Sea. Mar Ecol Prog Ser 266:15–25

Nausch M, Nausch G, Wasmund N, Nagel K (2008) Phosphorus pool variations and their relation to cyanobacteria development in the Baltic Sea: a three-year study. J Mar Syst 71:99–111

Nausch M, Nausch G, Mohrholz V, Siegel H, Wasmund N (2012) Is growth of filamentous cyanobacteria supported by phosphate uptake below the thermocline? Estuar Coast Shelf Sci 99:50–60

Nausch M, Achterberg EP, Bach LT, Brussaard CPD and others (2018) Concentrations and uptake of dissolved organic phosphorus compounds in the Baltic Sea. Front Mar Sci 5:386

Niemi Å (1979) Blue-green algal blooms and N:P ratio in the Baltic Sea. Acta Bot Fenn 110:57–61

Oksanen J, Simpson GL, Blanchet FG, Kindt R and others (2022) vegan: community ecology package. R package version 2.6-4. https://CRAN.R-project.org/package=vegan (accessed 12 July 2023)

Olofsson M, Suikkanen S, Kobos J, Wasmund N, Karlson B (2020) Basin-specific changes in filamentous cyanobacteria community composition across four decades in the Baltic Sea. Harmful Algae 91:101685

Passow U (2002) Transparent exopolymer particles (TEP) in aquatic environments. Prog Oceanogr 55:287–333

Peter KH, Sommer U (2013) Phytoplankton cell size reduction in response to warming mediated by nutrient limitation. PLOS ONE 8:e71528

Pitkänen H, Lehtoranta J, Räike A (2001) Internal nutrient fluxes counteract decreases in external load: the case of the estuarial eastern Gulf of Finland, Baltic Sea. Ambio 30:195–201

R Core Team (2022) R: a language and environment for statistical computing. R Foundation for Statistical Computing, Vienna

Raateoja M, Kuosa H, Hällfors S (2011) Fate of excess phosphorus in the Baltic Sea: A real driving force for cyanobacterial blooms? J Sea Res 65:315–321

Reynolds CS (2006) The ecology of phytoplankton. Cambridge University Press, Cambridge

Schneider B, Nausch G, Nagel K, Wasmund N (2003) The surface water CO_2 budget for the Baltic Proper: a new way to determine nitrogen fixation. J Mar Syst 42: 53–64

Schneider B, Gustafsson E, Sadkowiak B (2014) Control of the mid-summer net community production and nitrogen fixation in the central Baltic Sea: an approach based on pCO_2 measurements on a cargo ship. J Mar Syst 136:1–9

Simon M, Grossart HP, Schweitzer B, Ploug H (2002) Microbial ecology of organic aggregates in aquatic ecosystems. Aquat Microb Ecol 28:175–211

Sisma-Ventura G, Rahav E (2019) DOP stimulates heterotrophic bacterial production in the oligotrophic southeastern Mediterranean coastal waters. Front Microbiol 10: 1913

Solórzano L, Sharp JH (1980) Determination of total dissolved phosphorus and particulate phosphorus in natural waters. Limnol Oceanogr 25:754–758

Spilling K (2007) On the ecology of cold-water phytoplankton in the Baltic Sea. PhD dissertation, University of Helsinki

Spilling K, Markager S (2008) Ecophysiological growth characteristics and modeling of the onset of the spring bloom in the Baltic Sea. J Mar Syst 73:323–337

Spilling K, Olli K, Lehtoranta J, Kremp A and others (2018) Shifting diatom–dinoflagellate dominance during spring bloom in the Baltic Sea and its potential effects on biogeochemical cycling. Front Mar Sci 5:327

Spilling K, Asmala E, Haavisto N, Haraguchi L and others (2022) Brownification affects phytoplankton community composition but not primary productivity in eutrophic coastal waters: a mesocosm experiment in the Baltic Sea. Sci Total Environ 841:156510

Stigebrandt A, Rahm L, Viktorsson L, Ödalen M, Hall PO, Liljebladh B (2014) A new phosphorus paradigm for the Baltic proper. Ambio 43:634–643

Sundström AM, Kremp A, Tammilehto A, Tuimala J, Larsson U (2010) Detection of the bloom-forming cold-water dinoflagellate *Biecheleria baltica* in the Baltic Sea using LSU rRNA probes. Aquat Microb Ecol 61:129–140

Tanioka T, Matsumoto K (2020) A meta-analysis on environmental drivers of marine phytoplankton C:N:P. Biogeosciences 17:2939–2954

Turley CM, Newell RC, Robins DB (1986) Survival strategies of two small marine ciliates and their role in regulating bacterial community structure under experimental conditions. Mar Ecol Prog Ser 33:59–80

Turpin DH, Harrison PJ (1979) Limiting nutrient patchiness and its role in phytoplankton ecology. J Exp Mar Biol Ecol 39:151–166

Walve J, Larsson U (2007) Blooms of Baltic Sea *Aphanizomenon* sp. (Cyanobacteria) collapse after internal phosphorus depletion. Aquat Microb Ecol 49:57–69

Wasmund N (2017) Recruitment of bloom-forming cyanobacteria from winter/spring populations in the Baltic Sea verified by a mesocosm approach. Boreal Environ Res 22: 445–455

Wasmund N, Nausch G, Schneider B, Nagel K, Voss M (2005) Comparison of nitrogen fixation rates determined with different methods: a study in the Baltic Proper. Mar Ecol Prog Ser 297:23–31

Wasmund N, Nausch G, Voss M (2012) Upwelling events may cause cyanobacteria blooms in the Baltic Sea. J Mar Syst 90:67–76

Wickham H (2016) ggplot2: elegant graphics for data analysis. Springer-Verlag, New York, NY

Editorial responsibility: Robinson Fulweiler, Boston, Massachusetts, USA
Reviewed by: D. Rogers, A. Andersson

Submitted: April 5, 2023
Accepted: July 26, 2023
Proofs received from author(s): September 4, 2023